The thick, turbulent boundary layer on a cylinder: Mean and fluctuating velocities

Richard M. Lueptow, Patrick Leehey, and Thomas Stellinger
Massachusetts Institute of Technology, Cambridge, Massachusetts 02139

(Received 3 June 1985; accepted 29 August 1985)

The mean and fluctuating velocities in a turbulent boundary layer on a cylinder have been experimentally characterized for the case where the boundary layer is thick compared to the radius of transverse curvature. The mean velocity measurements suggest a mixed scaling for the "log law of the wall" using the wall coordinate yU_τ/ν and the ratio of the local boundary layer thickness to the radius of the cylinder δ/a. A relation for the slope and intercept of the log law of the wall as functions of δ/a based on empirical results and simple analysis is presented. Measurements of the Reynolds stress for δ/a of order 10 show that the Reynolds stress drops off much more quickly with distance from the wall than for a turbulent boundary layer on a flat plate. Both the Reynolds stress data and the turbulent intensity in the mean flow direction data are functions of the inverse radial distance from the center of the cylinder.

I. INTRODUCTION

This paper reports measurements of the mean velocity and Reynolds stress associated with the turbulent boundary layer that develops on the wall of a circular cylinder in axial flow. The measurements of the mean velocity profile reported in this paper are used along with results from other studies to propose an empirical model for the mean velocity profile in the turbulent boundary layer on a cylinder. This empirical model can be justified using a simple wake-like eddy viscosity closure. In addition, the present measurements include extensive results on the fluctuating velocities in the axisymmetric boundary layer for the case where the boundary layer is thick compared to the radius of the cylinder. Measurements of these fluctuating components of velocity have been largely neglected in previous studies. The present results for the fluctuation velocities provide insight into the distribution of turbulent quantities such as the Reynolds stress in an axisymmetric, turbulent boundary layer.

A number of serious attempts have been made toward a detailed experimental study of the mean properties of the axisymmetric, turbulent boundary layer. Several workers[1–5] have made measurements of the mean velocity profile on a cylinder with a small transverse curvature. The transverse curvature of the wall of the cylinder is usually characterized by the ratio of the boundary layer thickness δ to the radius of the cylinder a. For these studies, $\delta/a = O(1)$. However, as will be shown later in this paper, the effect of the transverse curvature is not significant unless $\delta/a > 1$.

Measurements of the mean velocity profile for $\delta/a > 1$ have been performed in four experimental studies. Willmarth *et al.*[6] made all measurements at a single axial station. Richmond,[1] Rao and Keshavan,[7] and Luxton *et al.*[8] made measurements at a limited number of axial stations. Patel *et al*[9] have characterized the mean velocity profile on a body of revolution. In this case, $\delta/a > 1$ only very close to the tail of the body of revolution.

A number of proposals for similarity laws have been suggested for the mean velocity profile in the turbulent boundary layer on a cylinder as a result of these experimental studies. These proposed laws are summarized in Table I. The fundamental difficulty in developing the similarity laws for the axisymmetric, turbulent boundary layer is the introduction of an additional length scale related to the transverse curvature of the cylinder, which is not present in the planar case. The logical choice for this transverse length scale is the radius of the cylinder a. Yet all the proposals for similarity laws outlined in Table I hinge on two fundamental questions.

First, what is the scaling parameter that results from the introduction of the transverse curvature a? The alternatives that have been proposed are $a_+ = aU_\tau/\nu$, δ/a, and $R_a = aU_\infty/\nu$. The first scaling parameter is an inner scaling based on the friction velocity U_τ and the kinematic viscosity ν. The second scaling parameter is a curvature ratio based on the boundary layer thickness δ. The third scaling parameter, a Reynolds number based on the free-stream velocity U_∞, mixes the inner transverse curvature with the outer free-stream velocity.

The second question centers on the effect of the transverse curvature on the fundamental character of the boundary layer. As the boundary layer thickness becomes small in comparison to the radius of curvature of the wall (perhaps $\delta/a \leqslant 1$), the boundary layer should become much like the boundary layer on a flat plate. Denli and Landweber[10] assert that as δ/a increases, the outer flow would likely be independent of the wall. This suggests a flow that is similar to a wake flow with a modified inner boundary condition.

Only one similarity law has been proposed for the sublayer, as shown in Table I. Rao[11] demonstrated that very close to the wall, where the viscous effects dominate, an inner scaling that preserves the linear form of the law of the wall is appropriate. Rao showed that in the viscous sublayer $U_+ = U/U_\tau = a_+ \ln(r/a)$, where $r = y + a$ is the distance from the center of the cylinder and U is the mean velocity.

The law of the wall and the velocity defect law are less obvious, as suggested by the number of proposals enumerated in Table I. All of the authors preserve the logarithmic form of the law of the wall. Yu[3] and Chin *et al.*[5] simply modified the coefficients of the flat plate law of the wall to

 0031-9171/85/123495-11$01.90

TABLE I. Proposals for similarity laws for the axisymmetric, turbulent boundary layer.

Author(s)	Sublayer	Law of wall	Outer law
Planar law	$U_+ = y_+$	$U_+ = A \ln(y_+) + B$ A,B,C,D universal	$(U_\infty - U)/U_\tau = C \ln(y/\delta) + D$
Richmond[1]		$U_+ = A \ln\{y_+[1 + (y/2a)]\} + B$ A,B universal	
Yu[3]		$U_+ = A \ln(y_+) + B$ A,C universal; B,D functions of R_a; L based on U_τ and ν	$(U_\infty - U)/U_\tau = C \ln(y/L) + D$
Rao[11]; Rao and Keshavan[7]	$U_+ = a_+ \ln(r/a)$	$U_+ = A \ln[a_+ \ln(r/a)] + B$ A,B functions of R_a, a_+	
Bradshaw and Patel[13]		$U_+ = A \ln\{4y_+/[1 + (r/a)^{0.5}]^2\} + B$ A universal; B function of a_+	
Denli and Landweber[10]		$U_+ = A \ln[a_+(r/a)^{0.5} \ln(r/a)] + B$ A universal; B function of a_+	$(U_\infty - U)/U_\tau = f(x/aR_a, y/\delta)$

account for the wall curvature. Chin *et al.*[5] also left the flat plate defect law intact except for changing the coefficients. Yu[3] modified the argument of the logarithm in the outer law from y/δ to y/L, where L is a length scale of the boundary layer based on the friction velocity and the kinematic viscosity.

Richmond[1] proposed replacing y_+ in the flat plate law of the wall with $y_+(1 + y/2a)$, based on Coles' streamline hypothesis.[12] Richmond did not alter the coefficients in the log law from those of the flat plate law, nor did he propose an outer law.

Rao[11] chose to preserve the form that comes about in the viscous sublayer by replacing the planar y_+ with $a_+ \ln(r/a)$. Later Rao and Keshavan[7] suggested that the coefficients for the law of the wall are functions of R_a and a_+. In the outer region they could not find any similarity based on y/δ or r_+.

Other modifications of the argument of the logarithm of the law of the wall have been based on mixing length arguments. Bradshaw and Patel[13] suggested changing the argument of the logarithm from y_+ to $\{4y_+/[1 + (r/a)^{0.5}]^2\}$ based on a mixing length argument. Denli and Landweber[10] proposed substituting $a_+(r/a)^{0.5} \ln(r/a)$ for y_+ in the argument of the logarithm based on a logarithmic mixing length model. They went on to propose a complicated defect law for the outer portion of the boundary layer based on its similarity to an axisymmetric wake for large δ/a.

In this paper we present a different law of the wall for an axisymmetric, turbulent boundary layer based on empirical results and simple analysis. The relation is somewhat simpler than the relations outlined above and appears to hold over a wide range of experimental conditions. As will be shown later in this paper, this law incorporates a mixed scaling dependent on the curvature ratio δ/a and the usual wall coordinates.

While the mean velocity profile has been experimentally characterized over a wide range of experimental conditions, far fewer experimental results have been presented for the fluctuating velocity components, which describe the fundamental turbulent nature of the axisymmetric boundary layer. For instance, the Reynolds stress has been measured for a cylinder with $\delta/a = O(1)$ by Afzal and Singh[4] and Chin *et al.*[5] and on a body of revolution by Patel *et al.*[9] No measurements of the Reynolds stress have been published for the case where the boundary layer thickness is much greater than the radius of transverse curvature. Other measurements of fluctuating components in the axisymmetric boundary layer include measurements of the turbulent intensity[8] and the fluctuating wall pressure[6] for $\delta/a > 1$.

In this paper we present experimental results related to the character of the fluctuating components of velocity in the axisymmetric boundary layer. In particular, measurements of the Reynolds stress for a curvature ratio of $\delta/a > 4$ are presented. These measurements provide some elementary understanding of the distribution of the turbulence in the axisymmetric boundary layer for large δ/a.

II. EXPERIMENTAL FACILITIES AND PROCEDURE

A. Wind tunnel and cylindrical model

The experiments described here were carried out in the Acoustics and Vibration Laboratory wind tunnel at the Massachusetts Institute of Technology. This open-circuit wind tunnel is shown in Fig. 1. It has a flow-straightening honeycomb at the inlet and a 20:1 contraction into the test section. The test section is 38 cm square and 3.7 m long. All experiments were performed at free-stream velocities between 12 and 40 m/sec. The level of free-stream turbulence in the wind tunnel was measured at less than 0.10% at these velocities.

The cylindrical model was suspended along the center line of the wind-tunnel test section. To prevent excessive sag of the cylinder in the horizontal wind tunnel, the cylinder was mounted in tension. It was anchored at the downstream end of the test section to a steel cross-shaped support attached to the wind tunnel superstructure. The cylinder

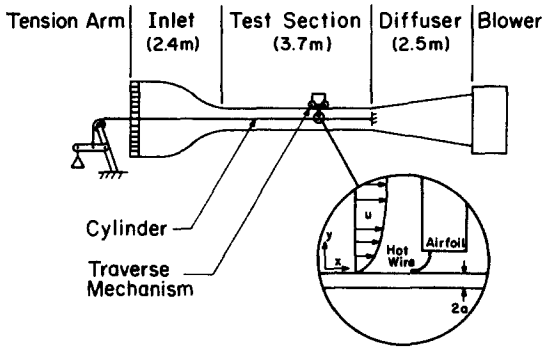

FIG. 1. Sketch of wind tunnel showing tensioning device, cylinder, and hot-wire traverse mechanism.

passed upstream along the tunnel axis and out through the honeycomb at the wind tunnel inlet. Here a cable attached to the cylinder passed over a pulley and was attached to a lever-arm tensioning device.

Two series of experiments, henceforth denoted series A and series B, were performed. In series A the cylindrical model was made from 0.15 cm (0.059 in.) diam spring steel music wire. The wire was placed under 1600 N (360 lb) tension, giving an estimated sag at the inlet of the test section (midpoint of the span of the wire) of 0.25 diam. In series B the cylindrical model was made from stainless steel tube 0.475 cm o.d. $\times$ 0.076 cm wall (0.187 in. o.d. $\times$ 0.030 in. wall). The tubing was placed under 1950 N (440 lb) tension. The sag, measured using a water level, was about 0.6 diam at the midpoint of the cylinder.

In series B, a 0.16 cm (1/16 in.) diam O-ring around the cylinder at the upstream end of the test section was used to trip the boundary layer. No boundary layer tripping mechanism was used in series A. In series A a portion of the inlet of the wind tunnel was partially blocked off using an open cell foam pad to correct for a slight transverse velocity gradient in the test section, which wiped the boundary layer off the cylinder. No modifications to the inlet were necessary for series B.

A slight favorable pressure gradient was measured in series B. This was caused by the acceleration of the flow as the boundary layers developed on the walls of the test section and the cylinder. The gradient was uniform along the length of the test section and the cylinder. The gradient was uniform along the length of the test section and was measured to be -10 Pa/m (-0.00043 psi/ft) at a free-stream velocity of 20 m/sec. In terms of the pressure coefficient, $C_p = 2\Delta P/\rho U_\infty{}^2$, the gradient was $dC_p/dx = -0.0004$/cm. It is unlikely that this very small favorable pressure gradient had a significant effect on the measurements reported here.

B. Instrumentation

Mean and fluctuating velocities were measured using U and X probes mounted in an airfoil that could be traversed along the length of the wind tunnel test section as shown in Fig. 1. Two streamwise traverse mechanisms were used. In series A a manual traverse on the bottom wall of the test section allowed the positioning of a hot-wire probe at any distance from the bottom of the cylinder at any location along the length of the test section. In series B a remotely controlled traverse on the top wall of the test section allowed the positioning of a hot-wire probe at any distance from the top of the cylinder at any location along the length of the test section.

Mean velocity profiles were measured in series A using a Thermo-Systems, Inc. 1261-10A hot-film probe with a sensor diameter of 0.0025 cm(0.001 in.) and a span of 0.025 cm (0.01 in.) The hot-film probe was used in conjunction with a Disa 55D05 constant temperature anemometer and a Disa 55D15 linearizer. The mean voltage output was measured on Disa 55D30 and Hewlett Packard HP40SCR digital voltmeters.

A modified Thermo-Systems, Inc. 1261 hot-wire probe was used to measure the mean velocity profiles in series B. The hot-wire probe was modified to reduce its sensing length and increase its spatial resolution. The sensing length was reduced to 0.07 cm (0.028 in.) by bending the prongs of the probe together and using a 2.5 μm (0.0001 in.) diam platinum–rhodium wire. This corresponds to $l/d = 280$ and $l_+ \approx 50$ at a free-stream velocity of 20 m/sec. According to an analysis presented in Ref. 14, the modification of the hot-wire probe should not have resulted in any excessive flow interference by the prongs. The modified hot-wire probe was used in conjunction with a Disa 55D05 constant temperature anemometer and a home-built linearizer. The mean voltage was measured with a Data Precision 1455 voltmeter. The rms fluctuating voltage was measured on a Bruel and Kjaer model 2607 measuring amplifier. In both series A and B the probes were calibrated against a pitot-static tube and a Betz micromanometer with a resolution of 0.1 mm H_2O.

The Reynolds stress was measured only in series B. A Thermo-Systems, Inc. 1249-T 1.5 X probe was used in conjunction with two Disa 55D05 constant temperature anemometers. The output from the anemometers was low-pass filtered at 5 kHz using Ithaco 4213 filters and then was sampled using a Hewlett Packard 2250 measurement and control unit. Since the HP2250 did not allow simultaneous sampling of the two channels, the signal was sampled at 20.8 kHz per channel. This minimized the delay time between corresponding samples on the two channels.

The X probe calibration scheme was based on directly measuring the voltage output of the X probe at different combinations of U and V velocities. To expose the X probe to different velocity components, the probe was situated at five different angles with respect to the mean flow in the wind tunnel. The voltage from each wire of the probe was measured at six different velocities for each angle. The velocity components were determined from the free-stream velocity and the angle of the X probe with respect to the free stream. The voltage readings and velocity components were used to generate a calibration grid using a method similar to that used by Willmarth and Bogar.[15] A Hewlett Packard 1000-A900 computer was then used to convert the raw voltages to velocity data from which the Reynolds stress was calculated. Because of the size of the X probe, the spatial resolution of

the X probe perpendicular to the surface of the cylinder was limited to 0.27 cylinder diam or about 90 viscous units at 20 m/sec.

For all boundary layer measurements the hot-wire probe was brought to within about 0.005 cm (0.002 in.) of the wall of the cylinder. The distance between the wall and the probe was measured with a microscope using a calibrated scale in the eyepiece. The hot-wire probe was moved away from the wall in steps of 0.0025 cm (0.001 in.) while recording the output of the hot-wire probe at each step. Further out in the boundary layer the steps were increased in size to a maximum of about 0.2 cm (0.078 in.). Typically, a mean velocity profile was determined from about 40 measurements.

Although attempts were made to minimize the error in the hot-wire measurements, some problems occurred. First, because of the time necessary to traverse the entire boundary layer thickness, the calibration drifted as much as 3%. A linear correction based on the calibration at the beginning and end of each test was applied to the data to account for this drift. Second, the linearizer used in mean velocity measurements allowed an accuracy only within 1%. No correction was applied for this error. Third, measurements near the wall of the cylinder were susceptible to misalignment of the center of the hot-wire probe with the center of the cylinder. Typically, this misalignment was obvious during an experiment and was corrected before recording any data.

C. Cylinder alignment and sag

Preliminary experiments and the experience of other researchers have suggested that the axisymmetric, turbulent boundary layer is susceptible to minor changes in the direction of the mean flow. This brings about two problems experimentally. First, misalignment of the axis of the cylinder with the mean flow may change the axial symmetry of the boundary layer. Second, the sag of the cylinder may locally change the axial symmetry of the boundary layer. Unfortunately, elimination of these experimental problems was impossible short of building a vertical wind tunnel. However, these effects were quantified in two different ways. In the first method, the axial symmetry was measured directly using a total head tube. In the second method, the cylinder was intentionally misaligned with the flow and the changes in the boundary layer profile were measured. These two methods are described in more detail below.

To directly measure the axial symmetry of the boundary layer on the cylinder, a 0.064 cm (0.025 in.) diam total head tube was mounted about 0.3 cm (1/8 in.) from the wall of the cylinder. The tube was mounted so it could slide and rotate on the cylinder. Before recording data, the upstream end of the cylinder was positioned so that the velocities measured using the total head tube were typically within 2% or 3% of one another at eight different circumferential positions. Although these variations in velocity are small, the change in the character of the boundary layer may be substantially larger. If a simple 1/7 power law is used to approximate the boundary layer profile, the effect of these small variations in velocity is estimated to produce a change in the boundary layer thickness on the order of 20%. The maximum measured circumferential difference in velocities was 5%, indicating even larger differences in the boundary layer thickness.

The overall alignment of the cylinder to the flow determines the axial symmetry of the boundary layer. To quantify the effect of flow alignment on the axisymmetric boundary layer, the cylinder was mounted at a slight angle with respect to the top and bottom walls of the wind tunnel test section while keeping it parallel to the side walls of the test section. The angle of attack of the cylinder with respect to the free-stream velocity is defined in Fig. 2(a) and represents the angle formed by the cylinder with respect to the top and bottom walls of the test section measured from the inlet of the test section to the downstream end of the cylinder. The angle of attack ϕ was estimated using a water level to measure the difference in height at these two locations. The angle of attack does not account for the slight sag of the cylinder between the inlet of the test section and the downstream end of the cylinder.

The thickness of the boundary layer as it develops along the length of the cylinder from the O-ring trip is shown in Fig. 2(a) for a free-stream velocity of 20 m/sec and three angles of attack. The data suffer from scatter attributable to errors mentioned in the previous section and the usual uncertainty encountered with the definition of the boundary

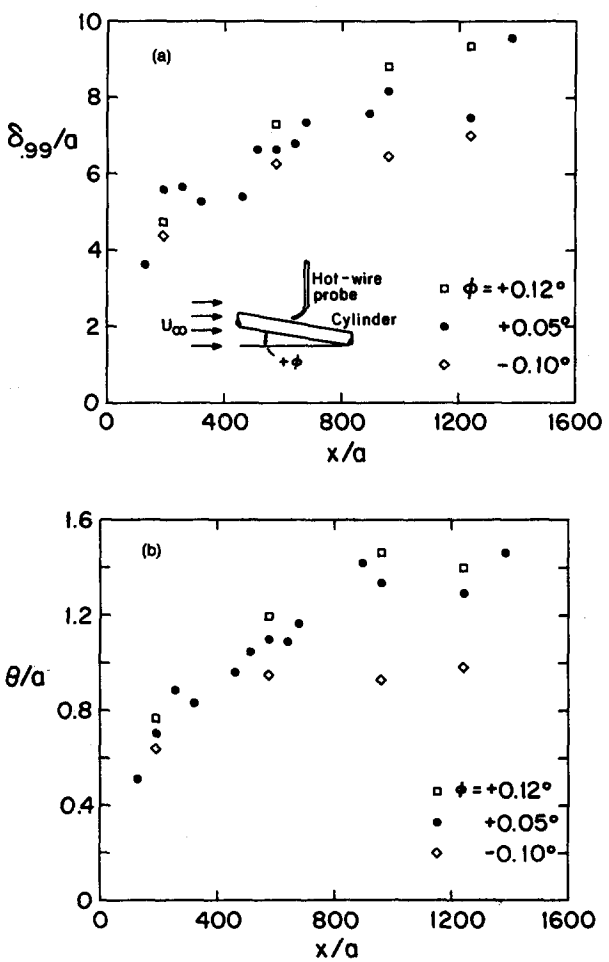

FIG. 2. Boundary layer development as a function of distance from trip x at 20 m/sec. (a) Boundary layer thickness $\delta_{0.99}$; (b) momentum thickness θ.

layer thickness. Nevertheless, the expected growth of the boundary layer is evident. However, the boundary layer thickness does not grow according to the law $\delta/a = 0.045(x/a)^{0.746}$ proposed by Afzal and Singh.[4] The difference is likely a consequence of the effect of the transverse curvature. Afzal and Singh used a large cylinder with $\delta/a = O(1)$. For the experiments described here δ/a is much larger.

As shown in Fig. 2(a) the boundary layer is thickened for a positive angle of attack and is thinned for a negative angle of attack. In other words, the boundary layer thickness measured on the leeward side of the cylinder with respect to the cross component of the flow ($\phi > 0$) is greater than the boundary layer thickness on the windward side of the cylinder ($\phi < 0$).

Although the sag of the cylinder and the angle of attack of the cylinder have been discussed separately up to this point, it is evident that they are not independent. The sag results in an effective local angle of attack that varies with the location along the length of the cylinder. Similarly, the angle of attack described up to this point is an overall measure of the misalignment of the cylinder with the flow. The effective local angle of attack is the sum of the local misalignment of the cylinder caused by the effect of sag and the overall misalignment of the cylinder caused by the flow being nonparallel to the axis of the cylinder.

The angles of attack shown in Fig. 2(a) are of the same order as the angles induced by the sag of the cylinder. This suggests that the sag may also be locally modifying the boundary layer thickness. If this were so, the boundary layer growth should tend to flatten moving from the midpoint of the cylinder downstream along the cylinder because of geometric considerations. For $\phi < 0$, ϕ becomes more negative with distance along the cylinder because of the curvature resulting from the sag of the cylinder. This would tend to thin the boundary layer toward the downstream end of the cylinder. For $\phi > 0$, ϕ decreases with distance along the cylinder because of the sag of the cylinder. This would tend to minimize the growth of the boundary layer toward the downstream end of the cylinder. Thus for either positive or negative ϕ the boundary layer thickness should not increase as quickly moving from the midpoint of the cylinder downstream along the cylinder as it would if there were no sag. The flattening of the boundary layer is not obvious in Fig. 2(a). However, the momentum thickness θ does appear to flatten for both positive and negative angles of attack moving downstream along the cylinder, as shown in Fig. 2(b). The displacement thickness (not shown) also flattens moving downstream along the cylinder.

Unless otherwise stated, $\phi \approx 0°$ for the experimental results described in the remainder of this paper. To minimize the effect of the sag in series B, the cylinder was mounted so that the height of the cylinder above the floor of the test section at the upstream end of the test section was the same as at the downstream end of the test section. Since the center of the length of the cylinder (where the sag is greatest) coincided with the upstream end of the test section, this meant raising the upstream end of the cylinder slightly compared with the downstream end. No similar correction for the sag was made in series A.

Of course, the boundary layer on the cylinder described here is not axisymmetric in a strict sense. In fact it is quite difficult to experimentally obtain a truly axisymmetric boundary layer considering the effects of the combination of sag and angle of attack. However, it will be shown later in this paper that these effects can be taken into account for both the mean and fluctuating components of velocity in a turbulent boundary layer on a cylinder.

III. RESULTS AND DISCUSSION

A. Mean velocity profile

Although a number of different similarity laws for the mean velocity profile in an axisymmetric, turbulent boundary layer have been proposed as shown in Table I, the results are presented here in terms of the traditional inner coordinates for the planar boundary layer. The reason for this will become apparent in the next section, where a mixed-scale log law is proposed.

The inner scaling yU_τ/ν requires the determination of the friction velocity U_τ. The most satisfactory method of finding the friction velocity is by the substitution of the experimental velocity profile U into the momentum integral relation for an axially symmetric boundary layer,

$$\left(\frac{U_\tau}{U_\infty}\right)^2 = \frac{d}{dx}\int_a^{a+\delta}\left[\frac{U}{U_\infty}\left(1-\frac{U}{U_\infty}\right)\left(\frac{r}{a}\right)\right]dr. \quad (1)$$

However, if the boundary layer is not axisymmetric, $U = U(r,\xi)$ and $\delta = \delta(\xi)$, where ξ is the azimuthal coordinate. Thus, substitution of the experimentally determined velocity profile U and boundary layer thickness δ measured on one side of the cylinder into (1) results in an inaccurate estimate of the friction velocity. Hence, unless perfect axisymmetry is maintained, this method of finding the friction velocity is inappropriate. In the experiments described here, the sag of the cylinder was large enough to cause an asymmetry of the boundary layer so that (1) could not be used for calculation of the friction velocity.

Instead of using (1), the friction velocity was determined by fitting the data to the buffer zone of Coles' law of the wall[12] for a planar boundary layer. The same method was used by Willmarth *et al.*[6] Of course, by using this method an implicit assumption has been introduced. The assumption is that very close to the wall the mean velocity profile of an axisymmetric boundary layer is no different than that of a planar boundary layer. Willmarth *et al.*[6] verified that this assumption is reasonable by comparing mean velocity profiles for axisymmetric boundary layers obtained by using a Preston tube to determine the friction velocity with Coles' law of the wall. For the region within the viscous sublayer and just above it, the mean velocity profiles matched Coles' law. However, later in this paper it will be shown that the friction velocities determined by matching data to Coles' law in the buffer region may be too large.

Using the friction velocity determined from matching Coles' law, the data were plotted in the usual flat plate wall coordinates, as shown in Fig. 3 for a free-stream velocity of 30 m/sec (series A). A family of curves results in the log region, with slopes slightly less than the slope for the planar

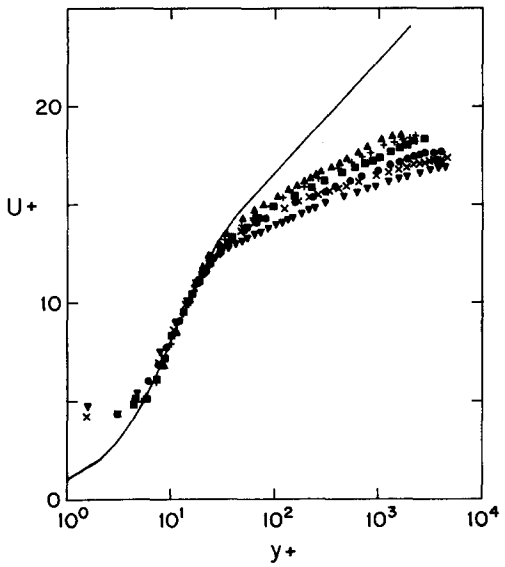

FIG. 3. Mean velocity profile, inner scaling (30 m/sec, series A). Solid line is Coles' law.

	▲	+	■	●	x	▼
δ/a	13.4	21.4	24.4	27.1	34.5	33.0
x/a	407	1220	2440	3051	3864	4271.

boundary layer. Similar families of curves result for free-stream velocities of 20 and 40 m/sec for series A and 12, 20, and 30 m/sec for series B. These results are not shown here for brevity.

In the family of curves shown in Fig. 3 the boundary layer thickness δ/a generally grows with streamwise location (see caption for Fig. 3). This growth is not without exception; note, for instance, $x/a = 4271$ where there is a slight decrease in the boundary layer thickness. We can only attribute this decrease to experimental error caused by sag or misalignment of the cylinder with the flow. Similarly, although not without exception, the slope of the log region of the velocity profile tends to decrease as the boundary layer thickens. Willmarth *et al.*[6] found a similar family of curves in which the slope of the log region of the velocity profile decreases as δ/a increases. However, unlike the results reported here, where the boundary layer thickness changed and the cylinder radius remained constant, the Willmarth *et al.* results were for different cylinder diameters at a single axial location. In both cases the slope of the log region of the boundary layer profile decreases as δ/a increases. This is the basis of the mixed-scaling logarithmic law of the wall proposed in the next section.

B. Proposed mixed-scale log law

The logarithmic portion of the velocity profile plotted in wall coordinates as in Fig. 3 suggests a log law of the form

$$U_+ = (1/m)\ln y_+ + n, \tag{2}$$

where

$$y_+ = yU_\tau/\nu.$$

Although the form of (2) matches the data in Fig. 3 for $y_+ > 50$, the coefficients in (2) are not constant and must somehow depend on the effect of the transverse curvature on the mean velocity in the boundary layer. Dimensional analysis suggests two scales based on the wall curvature: an inner scale a_+ and a curvature ratio scale δ/a. Dependence of m and n on a_+ can be ruled out since a_+ is only slightly different for all of the different log region slopes shown in Fig. 3. Hence, m and n must be functions of δ/a.

To justify the empirical equation (2), two cases must be considered. First, for a large cylinder where the effect of transverse curvature is small, a_+ is large and δ/a is small. Afzal and Narasimha[16] have derived an expression similar to (2) for this case, using the method of matched asymptotic expansions. For large $a_+ = aU_\tau/\nu$ and $\delta/a = O(1)$, they showed that m and n are constants.

The second case to be considered is that of a small cylinder, where a_+ is small and δ/a is large. In this case (2) can be justified using an eddy viscosity closure. In a planar boundary layer a constant stress layer occurs very close to the wall. In an axisymmetric boundary layer a similar analysis results in a constant stress moment near the wall, given by

$$r\tau = a\tau_w, \tag{3}$$

where τ_w is the shear stress at the wall and τ is the total shear stress given by

$$\frac{\tau}{\rho} = \nu\frac{\partial U}{\partial r} - \overline{uv}.$$

Using an eddy viscosity closure such that $\tau = \epsilon\, dU/dr$, and noting the definition for U_τ, (3) can be rewritten as

$$U_\tau^2 = \frac{r\epsilon}{\rho a}\frac{dU}{dr}. \tag{4}$$

For large δ/a the cylinder is so small that it should contribute little to controlling the eddy viscosity. In fact, a large "eddy" may pass from one side of a small cylinder to the other without even "seeing" the cylinder. Now a similar situation occurs in the outer region of a planar boundary layer where the wall does not control the eddy viscosity. This suggests that the eddy viscosity in an axisymmetric boundary layer may be like that for the outer region of a planar boundary layer. Further, Denli and Landweber[10] suggest that the axisymmetric boundary layer is much like an axisymmetric wake with a modified inner boundary layer for large δ/a. Now if the axisymmetric boundary layer has a wake-like character similar to the outer region of a planar boundary layer, then Clauser's estimate[17] for a constant eddy viscosity in the wake-like outer region of a planar boundary layer can be used. Thus $\epsilon = (c\rho\delta U_\tau)$, where c is some coefficient that is not yet known. Substituting into (4) results in

$$U_\tau = rm\frac{dU}{dr},$$

where $m = c\delta/a$. Now assuming c is independent of r, this can be integrated to yield

$$U_+ = (1/m)\ln r_+ + n, \tag{5}$$

where $r_+ = rU_\tau/\nu$. Now for small a_+, $\ln r_+$ is nearly the same as $\ln y_+$, reducing (5) to the form of (2), where m is the inverse of the slope of the log region and n is the intercept of the log region in Fig. 3.

Although this analysis requires several assumptions, it provides a crude analytical basis for the empirical log law (2). In addition, a functional dependence of the slope of the log law m on δ/a falls out of the analysis.

To test the dependence of the coefficients m and n on δ/a, m and n were obtained from a least-squares fit to the mean velocity profiles of series A and series B data as well as to the data of Richmond,[1] Chin *et al.*,[5] and Willmarth *et al.*[18] Of course some subjectivity is involved in deciding what constitutes a logarithmic region. In particular, the data of Willmarth *et al.* show a slight curvature of the logarithmic region, although the data are too sparse to justify anything other than a straight-line fit in the log region. However, this slight curvature of the log region suggests that the outer wake may be modifying the log region profile. The outer wake region may absorb the inner log region in a manner similar to the action of an adverse pressure gradient in a planar turbulent boundary layer.

The coefficients m and n calculated from the least-squares fit are shown in Fig. 4 as a function of δ/a. The scatter in the data, although substantial, is not surprising considering the subjectivity of the determination of m and n as well as the variety of wind tunnels, cylinder sizes, experimental methods, and free-stream velocities represented in Fig. 4.

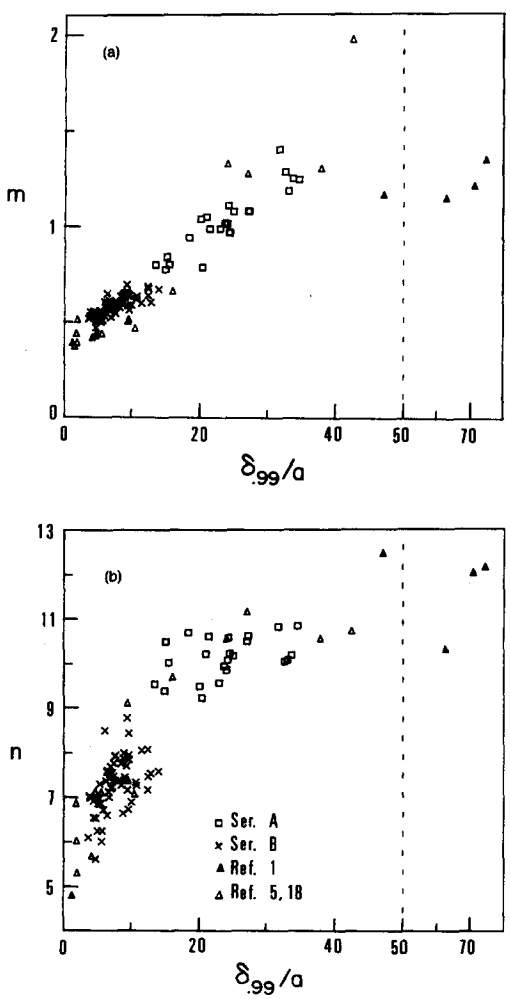

FIG. 4. Coefficients of the logarithmic portion of mean velocity profiles. (a) Inverse of slope m; (b) additive term n (Note the scale change at $\delta/a = 50$.)

Figure 4(a) shows that the inverse of the slope of the log region m is directly proportional to δ/a for $\delta/a < 40$, as predicted from the definition of m based on Clauser's estimate for a constant eddy viscosity. As the boundary layer thickness δ approaches the order of the transverse curvature a the inverse of the slope m nears the planar value of 0.4. The data for series B include m for several angles of attack ($\phi = -0.10°$, $\phi = 0.05°$, and $\phi = 0.12°$). Data for all angles of attack fall on the same line. Thus, m and n depend only on the local ratio δ/a independent of the asymmetry of the boundary layer because of sag or angle of attack.

For $\delta/a > 40$ the only data available are given by Richmond.[1] These data deviate substantially from the linear relationship for m as a function of δ/a. The deviation may be a result of experimental difficulties encountered by Richmond such as sag or alignment. These errors may have been particularly troublesome, since the data in question are for a cylinder of radius 0.03 cm (0.012 in.). On the other hand, the Richmond data may indicate a different turbulent flow regime for $\delta/a > 40$. Further experimental work on very small cylinders in axial flow will be necessary to clarify the situation for large δ/a.

The intercept n is large for large δ/a and decreases to the planar limit of 5.5 for $\delta/a = O(1)$ as shown in Fig. 4(b). In this case, though, the Richmond data fit in well.

From Figs. 4(a) and 4(b) the question of when the transverse curvature of the surface plays a role in determining the boundary layer profile can be answered. When the transverse radius of curvature of the cylinder is approximately the same as the boundary layer thickness, m and n approach their planar values, and the mean velocity profile is much like that of a flat plate. Thus, when $\delta/a = O(1)$ the effect of the transverse curvature is minimal with respect to the mean velocity profile. Afzal and Narasimha[19] also found that the boundary layer is effectively planar for $\delta/a \lesssim 1$.

Afzal and Narasimha[19] have used an asymptotic analysis to determine the functional dependence of m and n. They suggest that m and n are functions of $1/a_+$. However, the data they used to justify this dependence have no independent variation of a_+, as do the data presented here. The data shown in Fig. 4(a) do not collapse as well when plotted as a function of $1/a_+$ as when plotted as a function of δ/a. Thus, m and n seem to be functions of δ/a and not $1/a_+$.

C. Reynolds stress

The Reynolds stress $\overline{uv}$ in the turbulent boundary layer on a circular cylinder shows a distinctive departure from the planar Reynolds stress profile measured by Klebanoff,[20] as is shown in Figs. 5(a) and 5(b), when plotted in the usual planar outer coordinates. Here u and v are the fluctuating velocities in the streamwise and radial directions, respectively. Near the wall the axisymmetric Reynolds stress approaches the Reynolds stress for a flat plate. The Reynolds stress exceeds the planar value for a free-stream velocity of 20 m/sec [see Fig. 5(a)], possibly confirming the higher skin friction coefficient for an axisymmetric boundary layer predicted by Yu,[3]

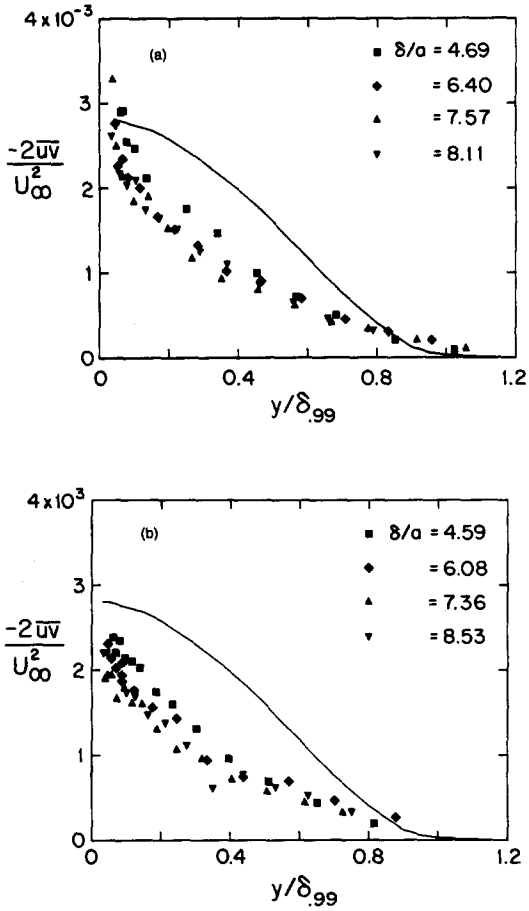

FIG. 5. Profile of Reynolds stress (series B). Solid line is the planar case.[20] The distance y is measured from the wall to the midpoint of the cross wires. (a) 20 m/sec; (b) 30 m/sec.

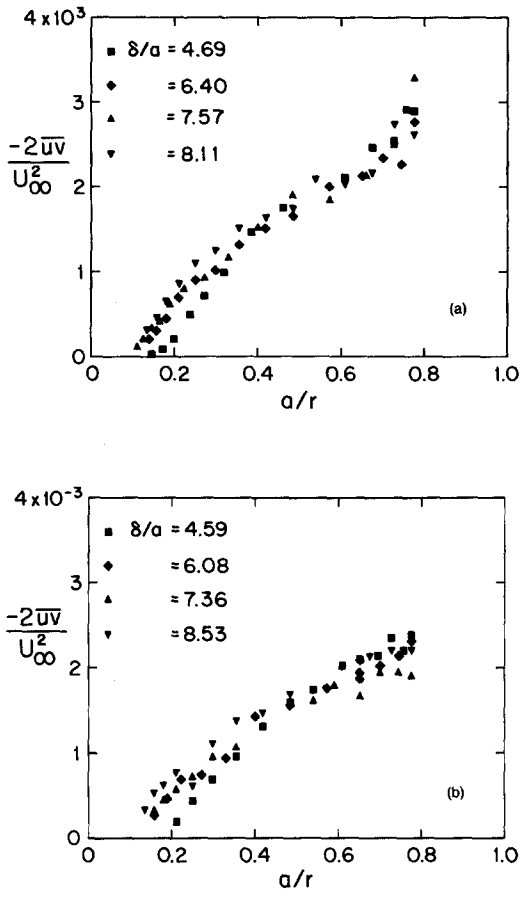

FIG. 6. Profile of Reynolds stress as a function of scaling a/r (series B). (a) 20 m/sec; (b) 30 m/sec.

Eckert,[21] and White.[22] This is not evident for a mean velocity of 30 m/sec [see Fig. 5(b)]. This may be caused by an inability to make Reynolds stress measurements very close to the wall at the higher free-stream velocity.

The overall shape of the Reynolds stress profile in the axisymmetric boundary layer is quite different from that for a flat plate. Moving away from the wall, the Reynolds stress drops off very quickly for the axisymmetric case compared to the planar case.

Before making any conclusions about the comparative shapes of the Reynolds stress profiles for the cylindrical and planar cases, the consequences of the equations of motion must be considered. In the planar case a constant shear region occurs near the wall. However, in the cylindrical case, a constant shear moment, Eq. (3), results from the equations of motion. Except for right at the wall, where viscous effects are important, the turbulent shear stress $\overline{uv}$ dominates the total shear stress. Thus, (3) can be written as

$$-\rho\,\overline{uv} = \tau_w(a/r). \tag{6}$$

Equation (6) indicates that the Reynolds stress should be a function of a/r near the wall. Such a representation is shown in Figs. 6(a) and 6(b). Except for the regions at the extreme values of a/r, the data collapse reasonably well onto a line throughout the boundary layer. Near the wall (large a/r) the failure of the data to collapse can be blamed on errors in the X-probe measurements near the wall. These errors include misalignment of the X probe over the cylinder and spatial averaging of the fluctuating velocities over the length of the hot wires.

At the outer edge of the boundary layer (small a/r), the data do not collapse because of the differences in the boundary layer thicknesses of the data sets represented in Figs. 6(a) and 6(b). However, there seems to be a trend of an increased Reynolds stress with increasing δ/a. If the Reynolds stress is plotted against the inverse radius scaled by the radius of the outer edge of the boundary layer, $r_\delta = \delta + a$, the data collapse quite well in the outer region of the boundary layer, as shown in Fig. 7. However, this scaling for r spreads the data in the region closer to the wall.

Figures 6 and 7 suggest how the Reynolds stress depends on distance from the cylinder for a turbulent boundary layer on a cylinder for $\delta/a = O(10)$. Near the wall the Reynolds stress is a function of an inner scale a/r. Away from the wall the Reynolds stress is a function of an outer scale r_δ/r.

The data shown in Figs. 6(a) and 6(b) can be used to show that the method of determining the friction velocities pre-

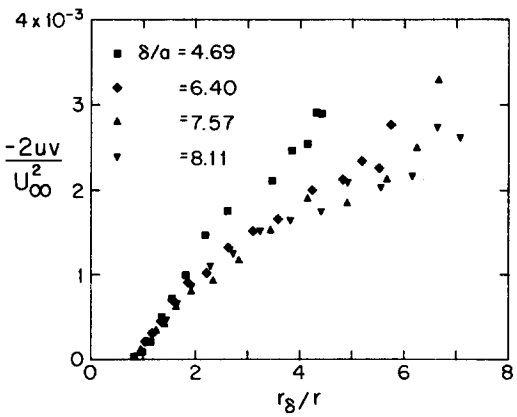

FIG. 7. Profile of Reynolds stress as a function of scaling r_δ/r at 20 m/sec (series B.)

sented earlier in this paper yields values that may be too large. Substituting $\tau_w/\rho = U_\tau^2$ into (6) and dividing by the square of the free-stream velocity results in

$$(-2\,\overline{uv}/U_\infty^2) = 2(U_\tau^2/U_\infty^2)(a/r).$$

Thus the slope of the data in Figs. 6(a) and 6(b) is related to the friction velocity U_τ. Table II shows the friction velocity calculated from the slope of the data in Fig. 6 for $(a/r) > 0.25$ (to omit the effects at the edge of the boundary layer). Table II also includes the friction velocity determined from matching the mean velocity profile to Coles' law. Note that in all cases the friction velocity calculated from Fig. 6 is less than that determined by fitting Coles' law. Since the analysis leading to the form of Fig. 6 omits inertial effects, the friction velocity calculated from the slopes may have some error. However, unlike matching to Coles' law to find the friction velocity, the slope method requires no assumption that the axisymmetric boundary layer is similar to the planar boundary layer.

The coefficients of the axisymmetric log law determined in the previous section were based on the determination of the friction velocity from fitting the data to the planar buffer region. Since the friction velocities calculated fitting to Coles' law may be too high, these results may be in question. However, a check of the effect of changes in the friction velocity of the magnitude suggested by determination of the friction velocity from the Reynolds stress data shows that changes in the coefficients $m(\delta/a)$ and $n(\delta/a)$ are within the scatter of the data.

TABLE II. Friction velocity calculated from slopes of Figs. 6(a) and 6(b) and from matching Coles' law (series B).

U_∞ (m/sec)	δ/a	x/a	U_τ/U_∞ (slope)	U_τ/U_∞ (Coles' law)
20	4.69	192	0.044	0.053
	6.40	576	0.040	0.051
	7.57	960	0.043	0.049
	8.11	1280	0.038	0.049
30	4.59	192	0.037	0.048
	6.08	576	0.039	0.046
	7.36	960	0.034	0.048
	8.53	1280	0.035	0.047

The Reynolds stress shown in Fig. 8 is nondimensionalized by the product of $u_{\rm rms} = \sqrt{(\overline{uu})}$ and $v_{\rm rms} = \sqrt{(\overline{vv})}$. Like the planar boundary layer[20] and turbulent channel flow,[23] the value of $\overline{uv}/u_{\rm rms}v_{\rm rms}$ is between 0.4 and 0.5 except near the wall and the outer edge of the boundary layer. Afzal and Singh[4] presented a similar result for an axisymmetric boundary layer with $\delta/a = O(1)$.

D. Streamwise turbulent intensity

The mean kinetic energy of the fluctuating motions in turbulence is given by

$$E_t = \tfrac{1}{2}\rho\,\overline{u_i u_i} = \tfrac{1}{2}\rho(\overline{uu} + \overline{vv} + \overline{ww}).$$

The largest contributor to E_t in shear turbulence is the streamwise turbulent fluctuation $\overline{uu}$. Although this quantity does not completely describe the mean kinetic energy of the fluctuating motions, it offers a reasonable approximation of the distribution of E_t in a boundary layer.

The scaling used for the distance from the wall for the Reynolds stress in the previous section is used in Fig. 9 to present the streamwise turbulent intensity $u_{\rm rms}$ for a free-stream velocity of 20 m/sec (series B). Plotting $u_{\rm rms}$ as a function of a/r collapses the data near the wall as shown in Fig. 9(a). At the outer edge of the boundary layer, $u_{\rm rms}$ is a function of r_δ/r as shown in Fig. 9(b).

Assuming that E_t acts in much the same way as its largest component, the fluctuating velocity in the direction of flow, it can be concluded that the total mean kinetic energy of the turbulent motions is a function of the same variables as the Reynolds stress. Near the wall the mean kinetic energy of turbulence is a function of a/r. Near the edge of the boundary layer it is a function of r_δ/r. Note that in Fig. 9 the data for $5.05 < \delta/a < 9.53$ all collapse to the same curve. So it appears that the functional dependence shown in Fig. 9 is independent of the transverse curvature for small changes in δ/a. Although it was not possible to show in Fig. 9 the data for various angles of attack ϕ, all collapse on the same curves.

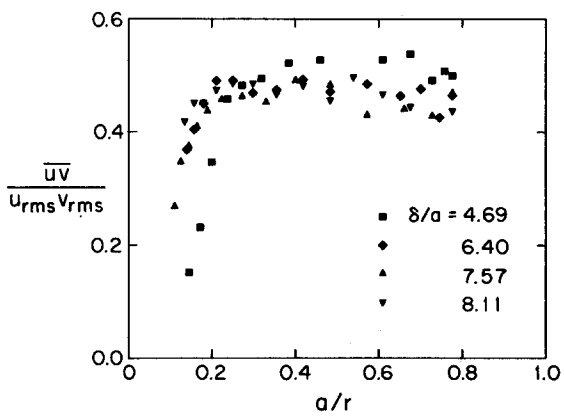

FIG. 8. Profile of Reynolds stress nondimensionalized by $u_{\rm rms}v_{\rm rms}$ as a function of scaling a/r at 20 m/sec (series B).

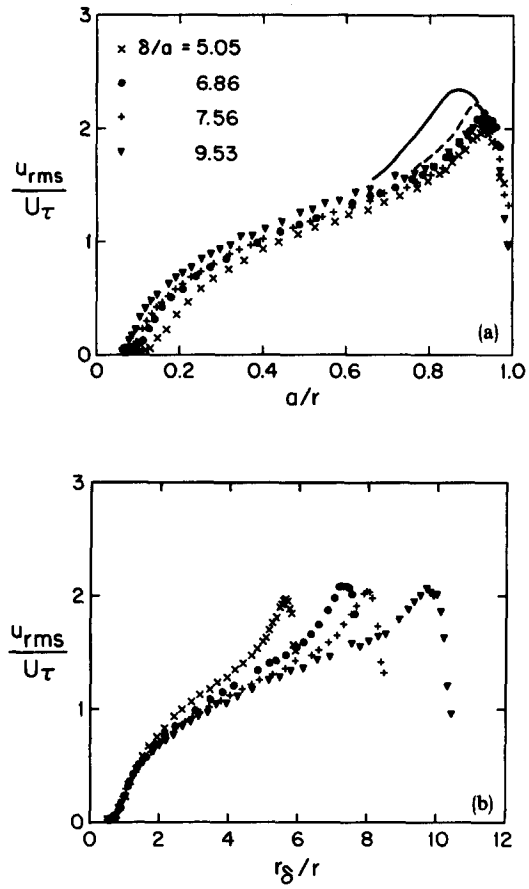

FIG. 9. Profile of streamwise turbulent intensity u_{rms} (series B, $\phi = +0.05°$). (a) As a function of a/r; (b) as a function of r_δ/r. Data points for 30 m/sec; 20 m/sec:-------; 12 m/sec:——.

Although near the wall the data appear to collapse based on a dependence on a/r, the location of the maximum u_{rms} differs depending on the free-stream velocity. This is shown in Fig. 9(a), which includes curves faired through data for free-stream velocities of 12 and 20 m/sec. Each curve shows a different radial location of the maximum u_{rms}. However, the maximum u_{rms} for all velocities occurs at a distance from the wall in viscous units of $y_+ \approx 16$. Thus, the maximum mean kinetic energy of the fluctuating motions in axisymmetric wall turbulence appears to be related to the distance from the wall measured in wall coordinates. This is nearly the same location of the maximum u_{rms} for the flat plate, which occurs at $y_+ \approx 15$ as estimated from Klebanoff's data.[20]

The magnitude of u_{rms} varies in Fig. 9(a) as a result of averaging the velocity fluctuations over the length of the hot wire. This is a result of different effective sensor lengths measured in viscous units because of different friction velocities. Willmarth and Sharma[24] found that, for a hot-wire length of $l_+ \approx 10$, about 10% of the rms velocity fluctuations could not be resolved. This effect may be even greater for the data in Figs. 9(a) and 9(b), since the hot-wire length ranged from $l_+ \approx 30$ for a free-stream velocity of 12 m/sec to $l_+ \approx 70$ for a free-stream velocity of 30 m/sec.

IV. CONCLUSIONS

The data presented in this paper show that a simple log law describes the mean velocity profile for a boundary layer on a cylinder. The relation (2) for the mean velocity profile is a log law based on mixed scales. It scales the distance from the wall of the cylinder with the traditional planar inner variable $y_+ = yU_\tau/\nu$. Unlike the planar boundary layer, though, the coefficients of the log law are not constants. Instead, these coefficients m and n depend on δ/a, a scale of the transverse curvature ratio. In fact, m is a linear function of δ/a for $\delta/a < 40$. Equation (2) accounts for local changes in the boundary layer thickness such as those resulting from a slight angle of attack of the cylinder with respect to the free-stream flow. As δ/a approaches, 1, the effect of the transverse curvature on the mean velocity profile is negligible, and the coefficients of the log law revert to their planar values.

Like other wall shear flows, the Reynolds stress nondimensionalized by $u_{rms}v_{rms}$ has a value between 0.4 and 0.5 except for near the wall and at the outer edge of the boundary layer. The Reynolds stress in the turbulent boundary layer on a cylinder nondimensionalized by the free-stream velocity is a function of the inverse radius measured from the center of the cylinder. Near the wall the radius is scaled by the radius of the cylinder. This functional dependence, predicted by assuming a constant stress moment near the wall, also holds for the streamwise turbulent intensity u_{rms}. In the outer region of the boundary layer, the inverse radius is better scaled by the radius of the outside edge of the boundary layer for both the Reynolds stress and the streamwise turbulent intensity.

The fundamental differences in the functional dependence of the turbulent quantities measured on a cylinder and a flat plate suggest that further work is necessary to understand the underlying mechanisms of turbulence. Work is currently under way in our facility to measure the details of the structure of the turbulence in a boundary layer on a cylinder. These measurements may yield information that will be helpful in further interpretation of the results presented in this paper.

ACKNOWLEDGMENTS

We are grateful to Dr. Joseph Haritonidis for sharing his extensive knowledge and expertise in hot-wire anemometry with us.

This work was supported by U. S. Office of Naval Research Contract No. N00014-78-C0696.

[1]See R. L. Richmond, AIP document no. PAPS PFLDA-28-3495-76 for 76 pages of California Institute of Technology Hypersonic Research Project Memo. No. 39 (1957). Order by PAPS number and journal reference from American Institute of Physics, Physics Auxiliary Publication Service, 335 East 45th Street, New York, NY 10017. The price is $1.50 for each microfiche (98) pages or $5.00 for photocopies of up to 30 pages, and $0.15 for each additional page over 30 pages. Airmail additional. Make checks payable to the American Institute of Physics.

[2]M. Yasuhara, Trans. Jpn. Soc. Aeronaut. Space Sci. 2, 72 (1959).
[3]Y. S. Yu, J. Ship Res. 2, 33 (1958).
[4]N. Afzal and K. P. Singh, Aeronaut. Q. 27, 217 (1976).

[5]Y. T. Chin, J. Hulsebos, and G. H. Hunnicut, *Proceedings of the 1967 Heat Transfer and Fluid Mechanics Institute* (Stanford University, Stanford, 1967), p. 394.
[6]W. W. Willmarth, R. E. Winkel, L. K. Sharma, and T. J. Bogar, J. Fluid Mech. **76**, 35 (1976).
[7]G. N. V. Rao and N. R. Keshavan, J. Appl. Mech. **39**, 25 (1972).
[8]R. E. Luxton, M. K. Bull, and S. Rajagopalan, Aeronaut. J. **88**, 186 (1984).
[9]V. C. Patel, A. Nakayama, and R. Damian, J. Fluid Mech. **63**, 345 (1974).
[10]N. Denli and L. Landweber, J. Hydronaut. **13**, 92 (1979).
[11]G. N. V. Rao, J. Appl. Mech. **34**, 237 (1967).
[12]D. E. Coles, *50 Jahre Grenzschictforschung* (Vieweg, Braunschweig, 1955), p. 153.
[13]P. Bradshaw, and V. C. Patel, AIAA J. **11**, 893 (1973).
[14]G. Comte-Bellot, A. Strohl, and E. Alcaraz, J. Appl. Mech. **38**, 767 (1971).
[15]W. W. Willmarth and T. J. Bogar, Phys. Fluids **20**, S9 (1977).
[16]N. Afzal and R. Narasimha, J. Fluid Mech. **74**, 113 (1976).
[17]F. H. Clauser, Adv. Appl. Mech. **4**, 1 (1956).
[18]See W. W. Willmarth, R. E. Winkel, T. J. Bogar, and L. K. Sharma, AIP document no. PAPS PFLDA-28-3495-136 for 136 pages of University of Michigan, Dept. of Aerospace Engineering, Report No. 021490-3-T (1975). See Ref. 1 for information on ordering.
[19]N. Afzal and R. Narasimha, AIAA J. **23**, 963 (1985).
[20]P. S. Klebanoff, NACA Report No. 1247 (1955).
[21]H. U. Eckert, J. Aeronaut. Sci. **19**, 23 (1952).
[22]F. M. White, J. Basic Eng. **94**, 200 (1972).
[23]P. H. Alfredsson and A. V. Johansson, J. Fluid Mech. **139**, 325 (1984).
[24]W. W. Willmarth and L. K. Sharma, J. Fluid Mech. **142**, 121 (1984).